The Environmental Effects of the April 2020 Wildfires and the Cs-137 Re-Suspension in the Chernobyl Exclusion Zone: A Multi-Hazard Threat

Rocío Baró, Christian Maurer, Jérôme Brioude, Delia Arnold, Marcus Hirtl

atmosphere

MDPI

Article

The Environmental Effects of the April 2020 Wildfires and the Cs-137 Re-Suspension in the Chernobyl Exclusion Zone: A Multi-Hazard Threat

Rocío Baró [1,*], Christian Maurer [1], Jerome Brioude [2], Delia Arnold [1,3] and Marcus Hirtl [1]

[1] Zentralanstalt für Meteorologie und Geodynamik, 1190 Vienna, Austria; christian.maurer@zamg.ac.at (C.M.); delia.arnold-arias@zamg.ac.at (D.A.); marcus.hirtl@zamg.ac.at (M.H.)
[2] Laboratoire de l'Atmosphère et des Cyclones (LACy), UMR8105, Université de la Réunion-CNRS-Météo-France, 97400 Saint-Denis de La Réunion, France; jerome.brioude@univ-reunion.fr
[3] Arnold Scientific Consulting, 08242 Manresa, Spain
* Correspondence: rocio.baro-esteban@zamg.ac.at

Abstract: This paper demonstrates the environmental impacts of the wildfires occurring at the beginning of April 2020 in and around the highly contaminated Chernobyl Exclusion Zone (CEZ). Due to the critical fire location, concerns arose about secondary radioactive contamination potentially spreading over Europe. The impact of the fire was assessed through the evaluation of fire plume dispersion and re-suspension of the radionuclide Cs-137, whereas, to assess the smoke plume effect, a WRF-Chem simulation was performed and compared to Tropospheric Monitoring Instrument (TROPOMI) satellite columns. The results show agreement of the simulated black carbon and carbon monoxide plumes with the plumes as observed by TROPOMI, where pollutants were also transported to Belarus. From an air quality and health perspective, the wildfires caused extremely bad air quality over Kiev, where the WRF-Chem model simulated mean values of $PM_{2.5}$ up to 300 $\mu g/m^3$ (during the first fire outbreak) over CEZ. The re-suspension of Cs-137 was assessed by a Bayesian inverse modelling approach using FLEXPART as the atmospheric transport model and Ukraine observations, yielding a total release of 600 $\pm$ 200 GBq. The increase in both smoke and Cs-137 emissions was only well correlated on the 9 April, likely related to a shift of the focus area of the fires. From a radiological point of view even the highest Cs-137 values (average measured or modelled air concentrations and modelled deposition) at the measurement site closest to the Chernobyl Nuclear Power Plant, i.e., Kiev, posed no health risk.

Keywords: wildfires; atmospheric transport modelling; Chernobyl; exclusion zone; radionuclides; Cs-137; TROPOMI

Citation: Baró, R.; Maurer, C.; Brioude, J.; Arnold, D.; Hirtl, M. The Environmental Effects of the April 2020 Wildfires and the Cs-137 Re-Suspension in the Chernobyl Exclusion Zone: A Multi-Hazard Threat. *Atmosphere* **2021**, *12*, 467. https://doi.org/10.3390/atmos12040467

Academic Editors: Kathrin Baumann-Stanzer and Mizuo Kajino

Received: 27 February 2021
Accepted: 1 April 2021
Published: 8 April 2021

1. Introduction

Over the last decades, there has been an increase in wildfires around the globe [1,2]. Climate change with higher temperatures and lower humidity, due to changing precipitation patterns and higher evaporation, is the main factor raising the fire risk which will be exacerbated with the years to come. Fire weather seasons have extended globally, across 25.3% of the Earth's vegetated surface [2], leading to an increase of global burnable area. Biomass burning (BB) is an important source of greenhouse gases and the emitted aerosols are a key factor of the global aerosol system [3]. Thus, wildfires may become even more problematic when a multi-hazard perspective is considered.

Due to the accident that occurred at reactor #4 of the Chernobyl Nuclear Power Plant (NPP) in 1986, there was a release of gases and aerosols containing an enormous amount of radioactive material [4]. Consequently, six million hectares of forest lands were polluted by radionuclides [5]. Kashparov et al. [6] provide a map showing the contamination for the Chernobyl Exclusion Zone (CEZ). The radionuclides accumulated in the contaminated areas can be mobilized in the combustion process and further on through the smoke plume

as a consequence of forest fires [7,8], and can thus not only affect the vicinity of the fires but also areas over long distances [9].

Evangeliou et al. [10] studied the status of the forested area within the CEZ and the effect of climate change on the wildfires. The authors stated that the forest area has increased after 1986 up to more than 70%, related to the absence of any measure for maintenance of the forests, which can lead to an uncontrolled growth of the vegetation [11]. Due to the lack of measures for maintenance of the forests together with the generally increased risk of wildfires, especially after the pronounced forest fires of 2010, there is a potential increase of the likelihood of long-distance transport of re-suspended radionuclides in smoke plumes [7,8].

Several papers studied the impact of wildfires in the CEZ [6,7,12–14]. In spring and summer 2015 there were two major wildfires occurring in the CEZ, where effective doses above 1 mSv/year in the CEZ were found and lower values in the rest of Europe [7]. Kuzmenkova et al. [15] also studied the effect of the 2015 fires over the Bryansk region (Western Russia) by analyzing the peat fires in the Bryansk region as the source of radioactive contamination. They found that the aerosols transferred horizontally via peat fires cannot reach beyond 500 m, so the radioactive particles found in the Bryansk region were not transported though peat fires.

According to information from the *Austrian Radioprotection Authority* (Federal Ministry for Climate Protection, Environment, Energy, Mobility, Innovation and Technology (BMK), Abt. V/8-Strahlenschutz, 8 April, personal communication), on the 4 April a wildfire broke out near the Chernobyl NPP in Ukraine. The *State Emergency Service of Ukraine* stated that a fire had started in the area near Volodumurivka village (Kotovske Forestry), in the Exclusion Zone of the Chernobyl NPP. Following the event, the *State Agency of Ukraine for the Management of the Exclusion Zone* set up a reinforced control of the radiological situation in the area of the exclusion and mandatory resettlement zone. According to [14], this fire was the largest one in the history of the CEZ and it therefore raised concerns with respect to its potential consequences. Although the wildfires were mostly declared extinguished by the 15 April, they became reactivated under the effect of strong winds which stirred up the embers of the recent fires [16]. Therefore, on the 17 April 2020, NASA's Terra satellite [17] captured new fires breaking out again in the CEZ and also starting outside the area. The fires lasted until the 20 April, spreading up to 80,000 hectares in the CEZ due to wind influence [14].

The aim of this work is to better understand the effects related to this significant wildfire event from two angles: (a) atmospheric transport modelling of the smoke plume and (b) estimating the potential radiological consequences following a source term estimation using inverse modelling techniques also in combination with atmospheric transport modelling. Cs-137 emissions in the present work are estimated using a Bayesian framework. Thus, this work complements other studies, such as [13] or [14] where Cs-137 emissions were estimated based on the use of diverse satellite observation products. Specifically, an improved determination of the burned area and estimation of the biomass combustion rate as a function of the retrieved fire radiative power (FRP) are key ingredients of such a satellite-based estimation.

2. Experiments

To assess the environmental impact of the fires, two different experiments were performed. In the first experiment, we used the Weather Research Forecast (WRF) coupled with the chemistry model (WRF-Chem) [18] to study the evolution of the smoke plume and compared it to the TROPOMI instrument total column data. TROPOMI images were obtained through the TOP platform [19]. In the second experiment, a Cs-137 source term estimation based on a Bayesian inversion using the FLEXPART [20] atmospheric transport model and observational data was performed to identify the possible radiological risk of Cs-137 spread.

2.1. WRF-Chem Wildfires Simulation

2.1.1. Set-Up of the WRF-Chem Simulation

The online-coupled chemical transport model WRF-Chem [18] simulates the emission, transport, mixing, and chemical reactions of trace gases and aerosols, as well as meteorological conditions. The WRF-Chem model (version 3.9.1) was run at a horizontal resolution of 12 km and at 47 vertical levels for the European domain. The following physical model options were used: the two-moment cloud microphysics scheme [21], Rapid Radiative Transfer Method for Global (RRTMG) long-wave and short-wave radiation [22], Grell 3D cumulus parameterization [23], NOAH land surface model [24], and the Mellor–Yamada–Nakanishi–Niino (MYNN) level 2.5 planetary boundary-layer (PBL) scheme [25].

WRF-Chem simulations were performed from the 4 to 11 April 2020. In WRF-Chem, external meteorological data are only used as initial and boundary conditions. For this study, these data were obtained from the European Centre for Medium-Range Weather Forecasts-Integrated Forecasting System (ECMWF-IFS) [26] every three hours with 0.25 horizontal resolution and at 137 vertical levels. In order to provide realistic initial conditions, an 8-day spin-up period was applied. The simulated variables shown in this study are black carbon (BC) and carbon monoxide (CO).

2.1.2. Wildfire Emissions

To perform a WRF-Chem wildfire simulation, we need to provide an additional input containing the wildfires emission data. In this study, the data came from the IS4FIRE Project [27], where emissions are estimated by reanalysis of fire radiative power (FRP) data obtained by the Moderate Resolution Imaging Spectroradiometer (MODIS) instrument (on board Aqua and Terra satellites). The IS4FIRE project provides emission files with 3D fluxes in kg/second for the total (primary + secondary) particulate matter (PM) derived from FRP. Three different particle sizes are considered:

- ems_PM_FRP_m_17: particulate matter with nominal diameter of 0.17 µm
- ems_PM_FRP_m1_1: particulate matter with nominal diameter of 1.1 µm
- ems_PM_FRP_m3_1: particulate matter with nominal diameter of 3 µm

The data are 3-hourly, with 0.1 × 0.1 degree spatial resolution and contain five stacked vertical layers. We computed the total particulate matter (PM) and interpolated to the regular grid to the WRF Lambert grid. Then, we calculated the different chemical speciation for aerosol (PM below 2.5 µm diameter, $PM_{2.5}$; PM below 10 µm diameter, PM10 and BC) following [28] and the gas speciation of CO. Figure 1 shows an example for the 8 April, 2020, of the fire emissions used; Figure 1a provides the emission intensity in kg/second of PM with a diameter of 1.1 µm, derived from the FRP, and Figure 1b the converted BC emission following the requirements for the NetCDF file that the WRF-Chem model needs as input.

The WRF-Chem model incorporates an online plume calculation able to compute the plume rise and release of biomass burning emissions based upon the simulated meteorology [29]. The prepared input data specifies the location of the fire and the amount of emitted species and the WRF-Chem model computes the plume rise of the wildfire smoke based upon the environmental wind and temperature profile. The forecast emissions are then provided as a vertical distribution based upon the results from the plume rise calculation. For more details, we refer the reader to [29,30].

2.1.3. Qualitative Satellite Analysis

In this study, we compared the simulated smoke plumes with TROPOMI total column data. This instrument is situated on board the Sentinel-5 Precursor satellite, the first Copernicus satellite dedicated to monitor the troposphere, and provides daily global information on concentrations of trace gases and aerosols at high spatial resolution (3.5 × 5.5 km). It carries the TROPOMI instrument with the main objective of performing atmospheric measurements [31]. TROPOMI was chosen due to its operational availability and high resolution to assess how well the smoke plume was simulated by the model.

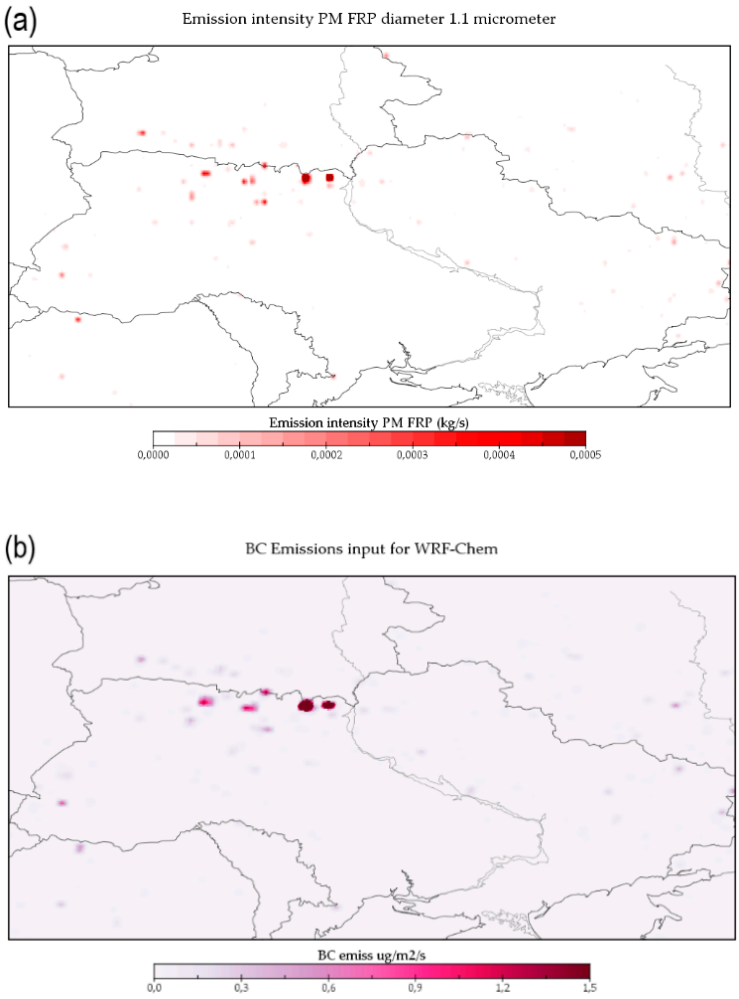

Figure 1. (**a**) Emission intensity of particulate matter (PM) in kg/second per grid with nominal diameter of 1.1 µm derived from the IS4FIRE project; (**b**) Black Carbon (BC) emissions ready to be used as input for the WRF-Chem simulation for the 8 April 2020.

2.2. Cs-137 Source Term Estimation and FLEXPART Simulation

2.2.1. Source Term Estimation of Re-Suspended Cs-137

Cs-137 Air Samples from Ukraine

On the 14 April 2020, the *State Nuclear Regulatory Inspectorate of Ukraine* (SNRIU) released 25 Cs-137 ambient activity concentration measurements taken at ground level at the stationary observation points (see Table 1 and also Figure 6) at Rivne NPP (RNPP), Khmelnitsky NPP (KhNPP), South-Ukraine NPP (SUNPP), Zaporizhzhia NPP (ZNPP) and at the Ukrainian Hydrometeorological Institute in Kiev. Out of the 25 samples, five were neglected because the sampling times mostly covered periods before the reported start of the fire and thus hardly the main period of interest (i.e., from the 4 to 11 April).

Set-Up of the Lagrangian Particle Dispersion Model FLEXPART

FLEXPART version 10.4 [20] was run driven by operational ECMWF-IFS [26] data with 0.2° horizontal resolution and 137 vertical hybrid levels covering the domain 25° W to 65° E and 30° N to 75° N. In order to largely suppress the forecast error, 12-hourly short-term forecasts launched at 00 and 12 UTC each day were concatenated. 20 Cs-137 samples with collection stops between the 6 April, 03:21 UTC, and 13 April, 06:00 UTC, were backtracked individually until the 4 April, 00:00 UTC using unit emissions and two million computational particles per sample (in total 40 million particles for the whole simulation) with species characteristics of aerosol bound Cs-137. FLEXPART synchro-

nization interval and output sampling rate was set to 900 s and averaging as well as the output time interval to 3600 s. Subgrid terrain effect and convection parameterization were enabled. A standard single aerosol particle diameter of 0.4 µm size was used to simulate medium range transport. In reality, a bimodal activity size distribution is likely to be found with one mode at 10 µm and another one at 0.4–0.7 µm, but an exact quantification of the aerosol activity size distribution is difficult to achieve [13] given that it depends on the burning conditions (the type of fire) and the radionuclide contamination in different parts of the ecosystem [14]. The FLEXPART hourly output was set to contain two separate source-receptor sensitivity (SRS) layers of 0–1000 and 1000–3000 m a.g.l for all time steps and grid boxes to capture the sensitivity to elevated emissions (see also next paragraphs. The output domain was chosen to be identical to the one of the computational domain, (the meteorological domain, respectively) with a horizontal resolution of 0.1°. For forward modelling of the dispersion of the emissions from the Chernobyl wood fire, a very similar set-up was used. The only difference was that the output was confined to one layer of 0–100 m a.g.l. where measurements were taken, and that the inverted emission profile with 6-hourly resolution (see Figure 5) was selected for the time period from the 4 April, 00:00 UTC, to the 12 April, 00:00 UTC. Due to the slightly varying sampling beginning and end times (see Table 1), the start and stop times were rounded up and down by at maximum 2.5 h when evaluating the forward run.

Table 1. List of 20 measured and modelled samples considered in the study. Sub-set of 13 samples is marked with asterisks. Largest (Kiev) measurements are marked in bold.

Site	Sampling Begin [UTC]	Sampling End [UTC]	Measured Activity Concentration [µBq/m^3]	Modelled Activity Concentration [µBq/m^3]—LS-APC Ref.	Modelled Activity Concentration [µBq/m^3]—Lognormal Ref.
RNPP (51.34° N, 25.86° E)	20200405 05:10 *	20200406 03:21 *	13.5	0.0	0.0
	20200406 03:21	20200407 03:05	61.1	5.7	5.8
	20200407 03:05 *	20200408 03:05 *	15.8	5.0	5.1
	20200408 03:05 *	20200409 03:11 *	12.7	0.2	1.4
	20200409 03:11	20200410 03:09	4.7	0.4	2.5
KhNPP (50.34° N, 26.64° E)	20200405 07:10 *	20200406 05:40 *	14.5	0.0	0.0
	20200406 05:40 *	20200407 07:00 *	42.5	37.8	49.7
	20200407 07:00	20200408 07:00	<3.2	10.3	9.5
	20200408 07:00 *	20200409 07:00 *	<1.7	0.2	0.8
	20200409 07:00 *	20200410 07:00 *	<1.7	0.5	3.2
	20200410 07:00 *	20200411 07:00 *	<2.7	0.0	0.0
	20200411 07:00	20200412 07:00	13.5	0.0	0.0
SUNPP (47.81° N, 31.22° E)	20200406 04:00 *	20200410 04:00 *	14.5	41.4	12.0
	20200407 04:00	20200413 04:00	49.5	26.3	32.7
ZNPP (47.51° N, 34.58° E)	20204007 03:20 *	20200410 08:11 *	<6.1	1.4	1.2
	20200409 07:40	20200410 07:41	<16	6.0	2.4
	20200406 05:31 *	20200413 06:00 *	8.5	3.2	3.8
Kiev (50.39° N, 30.53° E)	20200406 04:00 *	20200408 04:00 *	**65**	**52**	**46**
	20200408 04:00	20200409 04:00	**220**	**118**	**52**
	20200409 04:00 *	20200410 04:00 *	**470**	**556**	**408**

Source Term Inversion Applying Different Methods

Two well established source term inversion approaches were tested in the frame of this work. For both approaches FLEXPART SRS fields were used as a linearized model between emissions and related measurements. Given that zero measurements are important for discriminating periods of zero and non-zero emissions, measured values were set to zero in the subsequent inversion procedure if falling below the Minimum Detectable Concentration.

The first approach is a least-squares algorithm with adaptive prior covariance (LS-APC) [32]. The LS-APC is based on a Gaussian distribution of transport and emission flux errors. The LS-APC, however, does not require an error covariance matrix for the prior estimate to be defined. It calculates the unknown prior covariance within an iterative method adhering to the following constraints: (i) non-negativeness of all elements of the unknown emission, (ii) sparsity, i.e., the elements of the unknown emission are zero unless there is sufficient information, and (iii) smoothness, i.e., that rapid changes in the temporal profile are possible but rare.

The second approach is based on a least square algorithm assuming a lognormal distribution for transport and prior errors [33]. The assumption of lognormal distributions for any observations and surface fluxes is in closer agreement with reality than a Gaussian profile and implicitly prevents negative fluxes in the posterior estimates. The covariance matrix for the transport model error was assumed to be diagonal, with an error estimate of 40% of the observed activity concentration for the diagonal elements, reflecting the transport model error [34]. In addition, no prior information on emission fluxes was given also for this method and only the observations and related emission time periods with significant sensitivity values (SRS > 0.01% of the total SRS) were conserved. Thus, large peaks that compensate for time periods with very low SRSs are prevented by this constraint, which is introduced since there is no smoothness or sparsity constraint in the lognormal algorithm.

It is known that the posterior error covariance matrix from a least square method is unrealistically low [35]. To calculate the error in the posterior emission estimates, we applied a Montecarlo approach on the LS-APC and lognormal inversions. A random term that follows a Gaussian distribution with a standard deviation of 40% was applied for each SRS value to simulate the error in the transport model. This transport model error estimate is based on the results of an inter-comparison of Eulerian and Lagrangian models [36]. The posterior emission estimate error for the LS-APC approach was calculated using the standard deviation around the mean value of the posterior emission estimates from 300 inversions. The uncertainty for the lognormal inversion was based on a 68% posterior density interval between percentile 16 and 84, with the best estimate being the median of the distribution.

The main sources of uncertainties in the present inverse modelling approach are the transport model itself including the driving meteorological data and the exact emission location. In the case of the Chernobyl fire, the stack of the BB plume was lifted by the buoyancy of the heated air masses. Hence, it can be assumed that a surface emission will a priori generate an error in the atmospheric transport modelled between the source and the stations as it is known that the maximum likelihood of the BB plumes injection height is found near the local PBL height [37,38]. To estimate the injection height, the results of the global near-real-time Copernicus Atmospheric Monitoring Service (CAMS-NRT) [39] were employed which implemented BB emissions in 2019 using FRP observations from the NASA MODIS satellites [40] to quantify BB emissions as well as heat for the Global Fire Assimilation System (GFAS) inventory [41]. The daily injection heights for the Chernobyl fire were thus derived based on CAMS information. The bottom and top of the BB plumes were on average between 1000 and 3000 m a.g.l. for the whole period.

Hence, in order to study the sensitivity on different injection heights, the height was constrained (1) by calculating the SRS average between 0 and 3000 m a.g.l. and (2) by using the immediate FLEXPART output for 1000 to 3000 m. In both cases a well-mixed BB stack within those layers was assumed.

In addition, a precise location of the fire, at a resolution of $0.1^\circ \times 0.1^\circ$, was retrieved from CAMS-NRT. However, uncertainties in the wind speed and direction can shift the BB plume in space and time in the model compared to the reality and will likely generate a bias in the inverse model posterior estimate. Hence, the source location was constrained as (1) a single grid cell centered over the fire detected in CAMS-NRT and (2) nine grid cells centered over the fire, to take into account a spatial uncertainty in the source location

provided by the CAMS model. The latter also takes better into account the spread of fires across the CEZ.

Given the above considerations, LS-APC and lognormal results based on 1000–3000 m injection height and nine grid cells in the horizontal are considered as the reference runs (marked in italics in Table 2) The temporal resolution of the posterior emission estimates was finally reduced from one (temporal resolution of the FLEXPART run) to 6 h.

Table 2. Emission estimates together with errors in Gigabequerel (GBq) (1 GBq = 1×10^9 Bq) for the two different approaches, different assumed source locations, and a different number of involved samples. The LS-APC and lognormal reference results are marked in italics.

Total Emission Estimate (GBq)	1 Grid Cell, 1000–3000 m, 13 Samples	9 Grid Cells, 1000–3000 m, 13 Samples	*9 Grid Cells, 1000–3000 m, All Samples*	9 Grid Cells, 0–3000 m, All Samples	1 Grid Cell, 1000–3000 m, All Samples	1 Grid Cell, 0–3000 m, All Samples	Average
LS-APC	576 ± 139	472 ± 192	*635 ± 198*	959 ± 310	548 ± 188	713 ± 273	651 ± 217
lognormal	531 ± 169	519 ± 165	*527 ± 117*	763 ± 171	550 ± 141	742 ± 198	605 ± 160

3. Results

3.1. Results from WRF-Chem Simulation

The WRF-Chem simulation was compared with the Aerosol Index (AI) and CO from TROPOMI data. Figure 2 shows the comparison between the total column aerosol BC simulated by the WRF-Chem model (left column) and the AI from TROPOMI (right column). Figure 3 shows the comparison between the total CO column simulated by the WRF-Chem model (left column) and the total CO column from TROPOMI (right column). Regarding BC, during the 7 April (Figure 2a,d), due to the wind direction, the smoke plume could reach Belarus. On the next day (Figure 2b,e), due to the wind, a change in the plume direction is observed, in agreement with the satellite observations. Moreover, there seem to be two fire sources, however, in the TROPOMI images, only one main smoke plume is observed. On the 9 April (Figure 2c,f), the smoke plume direction changed again, and the two major fire sources remain. In this case, TROPOMI AI also shows the two fire sources combined, with an expanded smoke plume in an easterly direction. Concerning CO, we were able to compare directly the total column values and to use the same color bar (Figure 3). We can see that the total CO column simulated by WRF-Chem shows lower values over the non-fire pixels (0.025 mol/m^2 compared to around 0.035 mol/m^2). However, the values over fire pixels are in good agreement with the TROPOMI values, as in both cases we can see the dark red pixels (0.09 to 0.1 mol/m^2). The transport direction was also well captured for this pollutant, showing the same pattern as for BC. Several fire sources can be seen as well for the simulated CO (Figure 3a–c) and in this case, especially for the 8 and 9 April, most of the fire sources are reflected by the TROPOMI images.

Health

UNIAN [11] reported extremely poor air quality over the city of Kiev after the first wildfire outbreak. However, to the authors' knowledge, there is no Ukrainian daily data available publicly for air pollutant concentrations to be compared to our WRF-Chem results. However, we show in Figure 4 the mean values of Particulate Matter below 2.5 µm ($PM_{2.5}$) of diameter in the near surface layer over the studied period, as an indicator of the poor air quality observed after the first outbreak of the wildfires. Values greater than 300 µg/m^3 are found in the CEZ, but also greater than 50 µg/m^3 outside the CEZ.

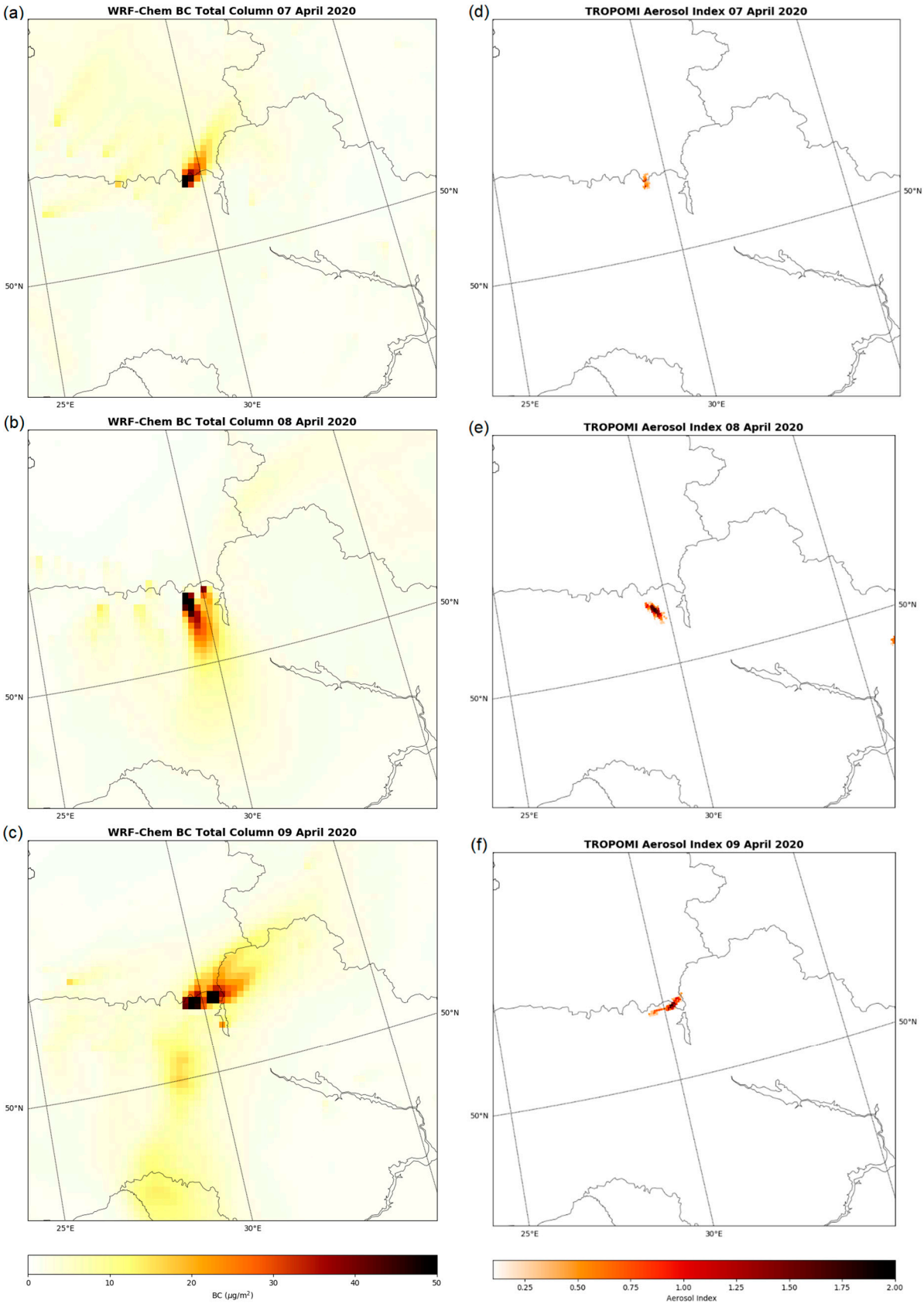

Figure 2. Simulated daily mean BC (μg/m^2) with WRF-Chem (**a**–**c**) and observed AI from TROPOMI (**d**–**f**) from the 7 to 9 April 2020.

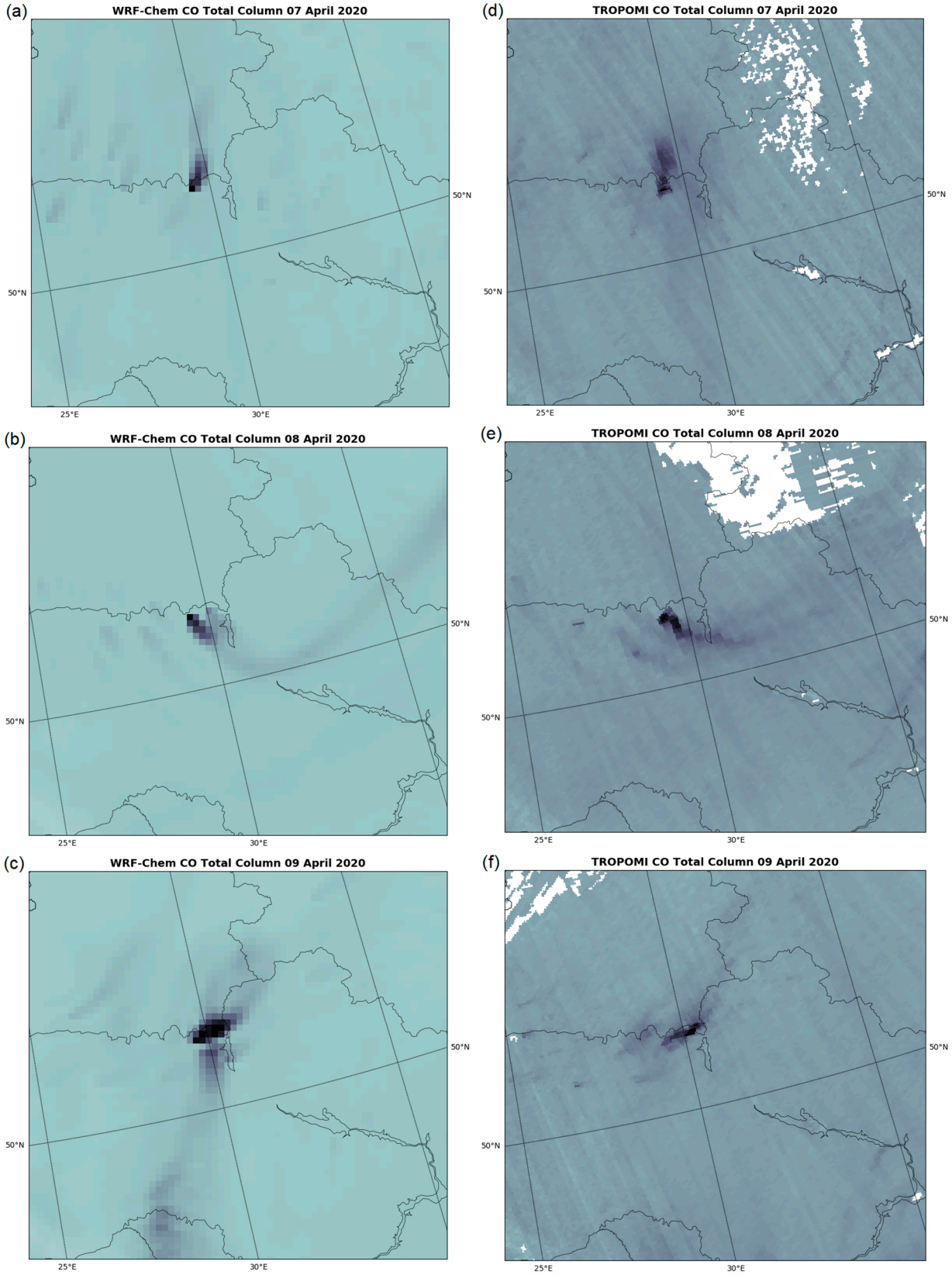

Figure 3. Simulated daily mean CO (mol/m^2) with WRF-Chem (**a**–**c**) and observed CO from TROPOMI (**d**–**f**) from the 7 to 9 April 2020.

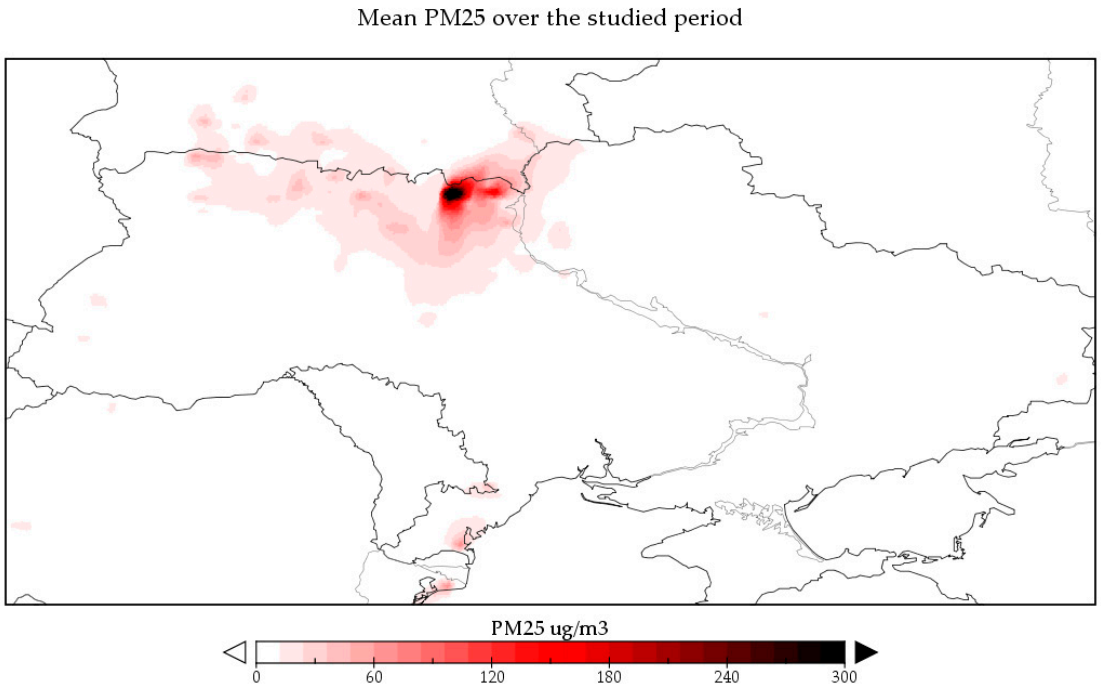

Figure 4. WRF-Chem mean $PM_{2.5}$ (ug/m^3) over the studied period.

3.2. Results for Cs-137 Source Term Inversion

The posterior estimates from the LS-APC and the lognormal approach (see Figure 5), for the different BB injection heights, surface area extensions of the source region, and number of involved samples all agree on a maximum release on the 9 April, between 00:00 and 06:00 UTC (403 and 309 GBq/6 h for the LS-ACP and lognormal reference runs). Figure 6a–c, showing the integrated Cs-137 activity concentration from the 4 until 9, 10, and 13 April, based on the reference LS-APC result (total emission of 635 GBq) reflects the major increase in emissions on the 9 April (magenta area north of Kiev). In fact, Kiev reported the highest measured activity concentrations on that day. Integrated concentrations (Figure 6) for the Kiev area are in good agreement with numbers recently published by [14] based on their atmospheric transport model LEDI (i.e., 250–350 Bqs/m^3 for the time frame 4 to 13 April). The emission profiles between the LS-APC and the lognormal approach differ with a smoother temporal variability in the LS-APC posterior than in the lognormal posterior due to the constraints in the iterative approach of the LS-APC method. Larger gaps in the lognormal posterior estimates are found due to the removal of time periods with very small SRSs at the assumed source location.

Although a validation with independent data should be performed in any study like this, this was not possible due to measurement data sparseness. It is evident from Figure 5 that when reducing the involved samples down to ~2/3 (13 instead of originally 20, marked with asterisks in Table 1), the number of gaps increases due to a lack of essential information (compare dashed and solid line in Figure 5). Thus, no independent samples could be explained with the inverted source term.

To make a crude, independent assessment of the estimated timing of the main emission, the emission profiles were compared to the daily CO flux product from the CAMS GFAS at 30.1° E/51.4° N for 8 to 11 April in the exclusion zone of the Chernobyl nuclear power plant. GFAS [41] assimilates fire radiative power (FRP) observations from satellite-based sensors to produce daily estimates of wildfire and biomass burning emissions and particularly CO. The CO flux shows an increase from the 8 to 9 April with a maximum on the 9 April 2020, which is in good agreement with the temporal trend of the estimated profiles of both the lognormal and LS-APC approach.

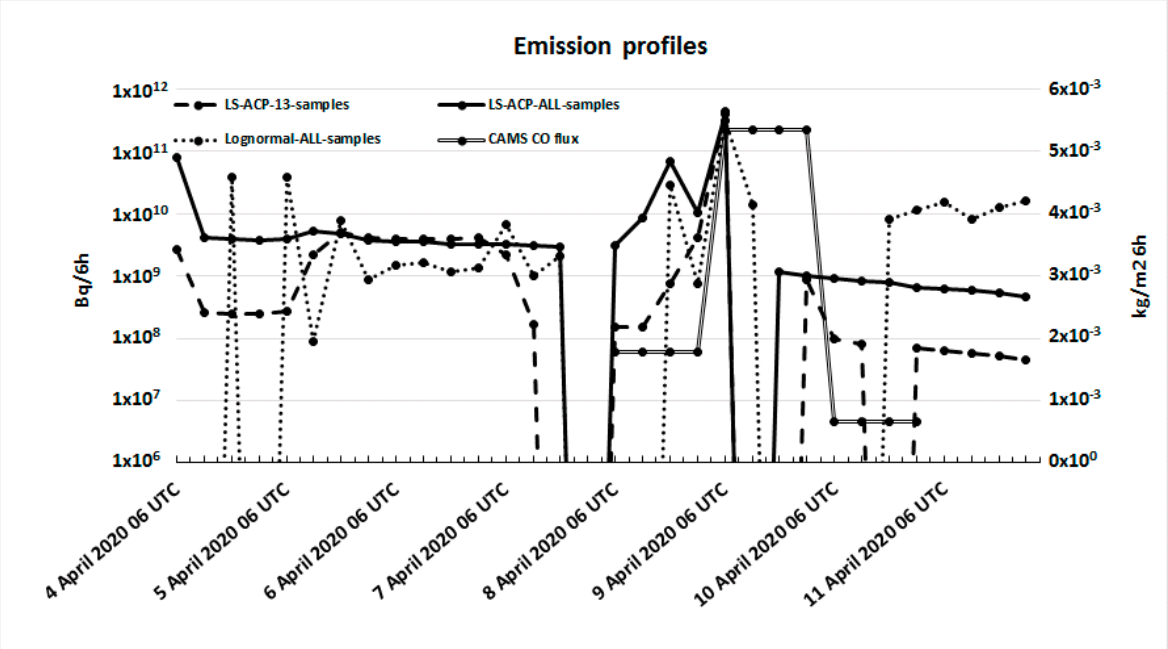

Figure 5. Cs-137 mission profiles (Bq/6 h) for the period 4 to 12 April resulting from the LS-APC and the lognormal approaches as well as the CAMS CO emission flux (kg/m^2 6 h) for 8 to 11 April. Source location was constraint to 1000–3000 m a.g.l. in the vertical and nine grid cells centered on the fire location according to CAMS. Zero emission values are not shown. Filled circles indicate the released activity, the total flux respectively, at the end of each six-hour period.

Dependent simulated observations based on both reference a posteriori estimates demonstrate that the LS-ACP algorithm, due to using Gaussian distributions, is dominated by the largest Kiev samples and thus reproduces them slightly better than the lognormal algorithm (see bold numbers in Table 1). The bias adds up to 6.7 and 17.6 µBq/m^3 for the LS-APC and the lognormal approach. Differences can also be found in the posterior total emission estimates (see Table 2). The emission estimates are ~7% lower for the lognormal approach than for the LS-APC approach (see last column with average values in Table 2). Error intervals overlap for every single inversion (see Table 2). The emission estimates increase by ~30 to 50% when an injection height of 0–3000 m is used instead of the reference interval of 1000–3000 m. The reason is that the plume injected below 1000 m will not efficiently affect the stations situated away from the source. Hence, the inversion compensates by increasing the emission flux at the source.

Finally, a simple consistency check was performed. Scaling of the three largest measurements from Kiev with the average above zero SRSs with respect to the Chernobyl NPP location yields a total release of 867 GBq for the time period from the 6 to the 10 April, which is in overall agreement with the results from the inversion. However, no time profile can be obtained with this simple approach.

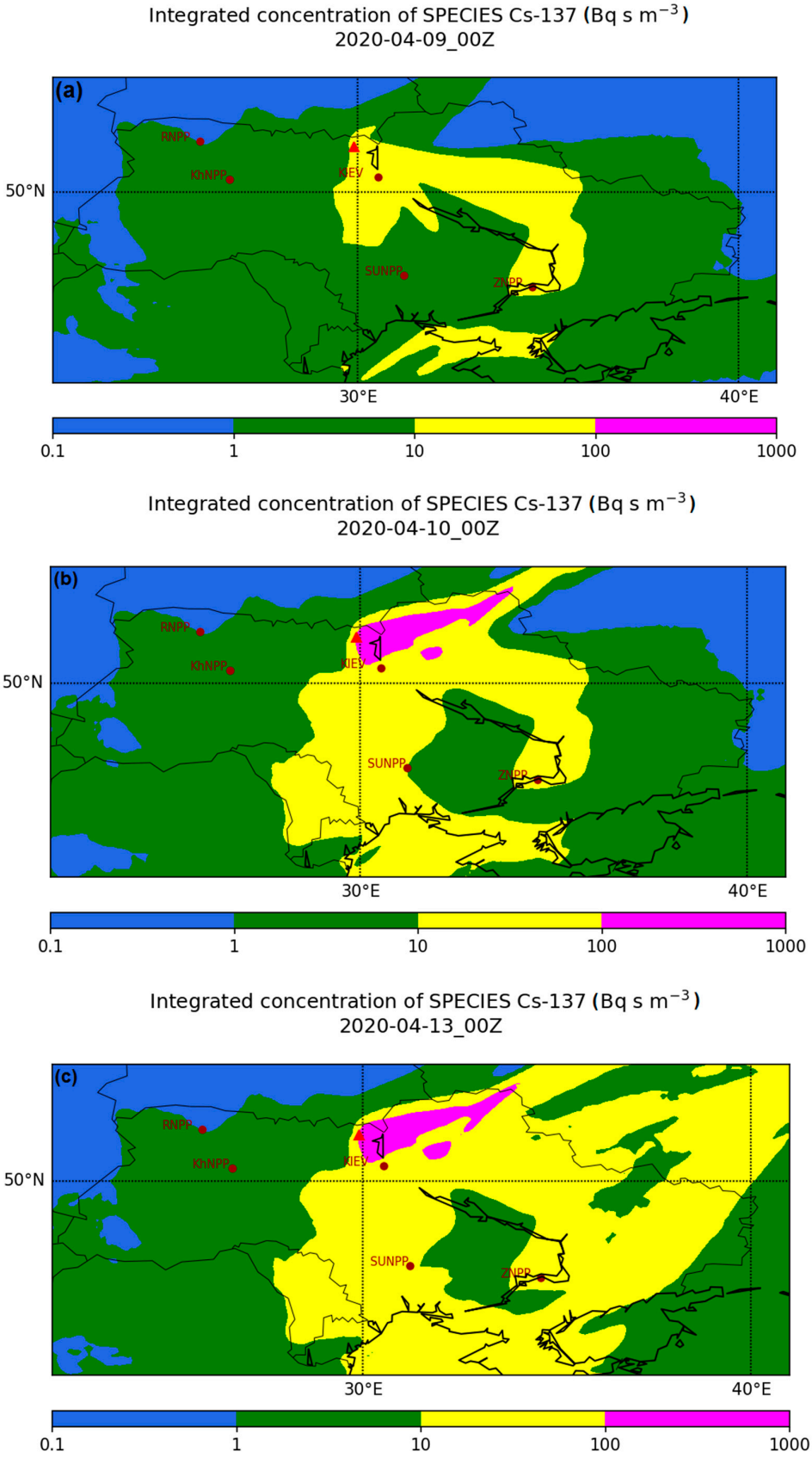

Figure 6. (**a**): Integrated Cs-137 activity concentration for the period 20200404 00:00 UTC to 9 April 2020 00:00 UTC. (**b**): For the period 4 April 2020 00:00 UTC to 10 April 2020 00:00 UTC. (**c**): For the period 4 April 2020 00:00 UTC to 13 April 2020 00:00 UTC. Red triangle indicates the source location.

4. Discussion

4.1. Discussion of the WRF-Chem Smoke Plume Simulation

In general, the WRF-Chem model can simulate the smoke plume since the results are in line with the data observed by TROPOMI. The aerosol BC was compared to the AI from TROPOMI, a direct value comparison was not possible to be done. Nevertheless, the highest BC values at and around the fire pixels coincide well with the satellite observations. On the other hand, CO values could be compared directly to the TROPOMI CO column values. As seen in Figure 3, the simulated WRF-Chem total column CO shows slightly lower values over the non-fire pixels, nevertheless, the fire pixels are in good agreement with the TROPOMI values. This has to be related to the fact that for the WRF-Chem simulation, only fire emissions were considered and not additional anthropogenic emissions. Therefore, the model shows lower CO levels where there is no fire. However, the WRF-Chem model run includes background contents for different chemical species, so the model does not start the run with zero background values. Regarding CO, there is a base value of 0.07 ppmv. The differences found in the background CO compared to TROPOMI data are around 0.01 $\mu g/m^3$ (35% difference). Nevertheless, the model captured the shift in wind direction, as seen in the evolution of the smoke plume (also for BC).

From an air quality point of view, several press releases [42–44] warned about the poor air quality due to the effects of the smoke plume after the first fire outbreak. The press releases reflected the Swiss monitoring group (IQAir) reporting information for the 17 April, where an Air Quality Index (AQI) of 380 for the city of Kiev can be found. This value can be compared to the levels in major polluted cities such a Shenyang in China, where the AQI was 180 on 17 April [42]. According to the United States *Environmental Protection Agency* (EPA) [45], values in the range of 151–200 are considered unhealthy. Therefore, the population was expected to be affected negatively by the AQI found in Kiev. There was no precipitation in the following days over Ukraine, leading to dry conditions, which may have kept the AQI levels high. Unfortunately, to the authors' knowledge, there is no daily data available publicly from air pollutant concentrations over the Kiev area to be compared with the present WRF-Chem results. The *State Statics Service of Ukraine* [46] provides environmental data, such as pollutant concentration, but currently, only data until 2019 is released. However, Figure 4 shows the modelled $PM_{2.5}$ mean values, indicating significantly high values. According to the *European Air Quality Directive* (2008/EC/50) [47] for the protection of human health, the PM10 (which includes the $PM_{2.5}$) daily mean value may not exceed the 50 $\mu g/m^3$ limit more than 35 times a calendar year. Therefore, the fires may have contributed significantly to exceed this threshold, due to their duration, exposing a health impact to the population.

4.2. Discussion of Source Term Estimation Using Inverse Modelling and Radiological Exposures

Overall, the two inversion methods yield fairly consistent results. No conclusion can be drawn as to whether the LS-ACP method or the lognormal method performs better. The largest Kiev samples may be reproduced slightly better based on the LS-ACP method, but better reproduction of the largest samples does not necessarily mean that the LS-APC based overall source term is more reliable than the lognormal based overall source term. The overall source terms compare well to the total Cs-137 emission provided by [48] for the period 4 to 12 April and by [13] for the period 1 to 22 April (~380 GBq and ~341 GBq, respectively, of Cs-137 were emitted according to these authors). The French Institute for Radioprotection (IRSN), however, states a range of 200 to 700 GBq according to [13]. In agreement with our study, the latter authors found a peak emission on the 9 April. This does not come unexpectedly. As can be seen from Figure 2 the focus of the fires evidently shifted to the Chernobyl NPP from 7 to 9 April thus affecting the most contaminated area (see also [14]).

The emission numbers can also be compared with an upper bound estimate based on the area of the CEZ and levels of contamination. According to a *United Nations Scientific Committee on the Effects of Atomic Radiation* (UNSCEAR) report [4] Cs-137 deposition levels

in the exclusion zone added up to 1500–3700 kBq/m^2. Taking into account that half of the Cs-137 has decayed after 30 years, assuming a fire covering the whole exclusion zone with 30 km radius around the NPP corresponding to 2.8×10^9 m^2 (282,743 ha) and an average deposition of 2×10^6 Bq/m^2 (2000 kBq/m^2), the total activity is equal to 2.8×10^{15} Bq. Assuming further a re-suspension rate of 1% [9] for Cs-137, the maximum source term would be 2.8×10^{13} Bq, i.e., 28000 GBq. Results of this study clearly fall far below this upper bound.

From a radiological point of view, the highest 24 h average measurement of 470 µBq/m^3 Cs-137 at the measurement site closest to the Chernobyl NPP (i.e., Kiev) poses no health risk even if it would have occurred over a period of several days. Using an inhalation rate for adults of 2.6×10^{-4} m^3/s, an effective inhalation dose coefficient for Cs-137 for adults of 4.6×10^{-9} Sv/Bq and an effective cloud shine dose coefficient for Cs-137 for adults of 2.55×10^{-14} Sv m^3/Bq s [49], yields 2×10^{-6} µSv/h or 4.5×10^{-4} µSv, i.e., 0.45 nSv, over nine days (from the 4 to the 13 April) of the fire event. A dose equivalent to an arm X-ray (1 µSv) would require roughly an activity concentration level of 1 Bq/m^3 over the nine days if only Cs-137 is involved. Comprehensive dose calculations based on atmospheric transport modelling results and including ground shine dose contributions vary largely for the 2020 forest fires in the CEZ as recently demonstrated by [13] and [14]. The main reason is likely the discrepancy in transuranic isotope (Pu-238 to 240 and Am-241) emission parameterizations, but uncertainties may also arise due to the size distribution of radioactive aerosols. They, in turn, determine deposition estimates (which vary for Cs-137 between 2.25 Bq/m^2 and 0.3 mBq/m^2 as estimated in the two publications mentioned above based on the atmospheric transport models LEDI and FLEXPART for the Kiev area). According to our FLEXPART simulation an overall total Cs-137 effective dose of 0.1 nSv at Kiev has to be expected, with 56 mBq/m^2 total deposition and an effective ground shine dose coefficient for Cs-137 for adults of 5.51×10^{-16} Sv m^2/Bq s.

The increases in both smoke plume and Cs-137 emissions are only well correlated on the 9 April. The increase in smoke emissions on 7 and 8 April, is not reflected in Cs-137 releases, which may be related to the position of the fires gradually affecting different parts of the CEZ. However, Cs-137 air samples are confined to five sampling sites and to Ukrainian territory, which implies that only part of the Cs-137 emissions may have been captured by any inversion approach. It is evident from the smoke plume (Figure 2, upper panel) that the smoke was also transported to Belarus.

5. Conclusions

In this paper, we studied the effects of the first outbreak of the most recent wildfires that occurred over the CEZ in April 2020, considering the spread of re-suspended Cs-137 and the smoke plume of the wildfires, and whether they posed a health threat, from a radiological view and due to the smoke plume. Cs-137 emissions in the present work were estimated using a Bayesian framework, thus this work complements other recent studies, such as [13] or [14] where Cs-137 emissions were estimated based on the use of diverse satellite observation products.

To assess the smoke plume impact, a WRF-Chem simulation was performed and qualitatively compared to TROPOMI data. Simulated BC and CO are in agreement with the plume as observed by TROPOMI, and during the 7 April it was transported to Belarus. Moreover, the model captured the shift in wind direction, as seen in the evolution of the smoke plume compared to the observed satellite total column values. Since only fire emissions were taken into account in the simulation, the non-fire pixels of the modelled CO showed lower values compared to TROPOMI. However, the fire pixels are in good agreement with the TROPOMI values. From an air quality perspective, the wildfires caused extremely bad air quality, with Kiev being one of the most polluted cities (after the first fire outbreak), compared to other major polluted world cities. The modelled $PM_{2.5}$ values showed a high concentration of this pollutant that led to very poor air quality and may

have contributed to exceeding the PM10 daily mean value limit of 50 $\mu m/m^3$, over several days, due to the duration of the fires, exposing a health impact to the population.

Re-suspension of Cs-137 was assessed by a FLEXPART inverse modelling approach. A total emission of about 600 $\pm$ 200 GBq was estimated with 350 GBq being emitted within a six-hour interval on early 9 April. However, since Cs-137 air samples are limited to sampling sites in the Ukraine, only part of the Cs-137 emissions may have been captured by any inversion approach. From a radiological point of view neither measurements nor modelled values of Cs-137 at the measurement site closest to the Chernobyl NPP, i.e., Kiev, posed a health risk. In contrast to radiation, air pollution was health relevant, which is in clear contrast to the general public perception.

Author Contributions: Conceptualization, R.B., C.M. and M.H; methodology, R.B., C.M., J.B. and D.A.; validation, C.M., J.B. and D.A.; formal analysis, R.B., C.M., J.B.; data curation, C.M., J.B. and R.B.; writing—original draft preparation, R.B., C.M.; writing—review and editing, R.B., C.M.; project administration and funding acquisition M.H. All authors have read and agreed to the published version of the manuscript.

Funding: This research was funded by the Oesterreichische Forschungsfoerderungsgesellschaft (FFG), grant number ASAP 13 in the frame of the project "Innovative APPlications for the augmented use of satellite observations to support Air Quality management" (APP4AQ).

Institutional Review Board Statement: Not applicable.

Informed Consent Statement: Not applicable.

Data Availability Statement: Cs-137 data was obtained from SNRIU and are available from the authors with the permission of SNRIU. Publicly available TROPOMI datasets were analyzed in this study. This data can be found here: http://top-platform.eu/ access on 1 April 2021.

Acknowledgments: We would like to thank the State Nuclear Regulatory Inspectorate of Ukraine (SNRIU) for officially granting the authors to use Cs-137 data as provided by SNRIU via the IAEA-USIE system in April 2020. We acknowledge the Copernicus Sentinel data 2020, processed by the TOP platform (http://top-platform.eu/ accessed on 26 March 2021). The CO profile information was generated using Copernicus Atmosphere Monitoring Service Information (https://apps.ecmwf.int/datasets/data/cams-gfas/ accessed on 22 March 2021).

Conflicts of Interest: The authors declare no conflict of interest. The funders had no role in the design of the study; in the collection, analyses, or interpretation of data; in the writing of the manuscript, or in the decision to publish the results.

References

1. Liu, Y.; Stanturf, J.; Goodrick, S. Trends in global wildfire potential in a changing climate. *For. Ecol. Manag.* **2010**, *259*, 685–697. [CrossRef]
2. Jolly, W.M.; Cochrane, M.A.; Freeborn, P.H.; Holden, Z.A.; Brown, T.J.; Williamson, G.J.; Bowman, D.M.J.S. Climate-induced variations in global wildfire danger from 1979 to 2013. *Nat. Commun.* **2015**, *6*, 7537. [CrossRef]
3. Lin, N.-H.; Sayer, A.M.; Wang, S.-H.; Loftus, A.M.; Hsiao, T.-C.; Sheu, G.-R.; Hsu, N.C.; Tsay, S.-C.; Chantara, S. Interactions between biomass-burning aerosols and clouds over Southeast Asia: Current status, challenges, and perspectives. *Environ. Pollut.* **2014**, *195*, 292–307. [CrossRef]
4. UNSCEAR: UNSCEAR 2000 Report, Vol. II, ANNEX J: Exposures and Effects of the Chernobyl Accident. p. 460. Available online: http://www.unscear.org/docs/reports/annexj.pdf (accessed on 27 August 2020).
5. Dusha-Gudym, S.I. Transport of radioactive materials by wildland fires in the Chernobyl accident zone: How to address the problem. *Int. For. Fire News* **2005**, *32*, 119–125.
6. Kashparov, V.; Lundin, S.; Khomutinin, Y.; Kaminsky, S.; Levchuk, S.; Protsak, V.; Kadygrib, A.; Zvarich, S.; Yoschenko, V.; Tschiersch, J. Soil contamination with 90Sr in the near zone of the Chernobyl accident. *J. Environ. Radioact.* **2001**, *56*, 285–298. [CrossRef]
7. Evangeliou, N.; Zibtsev, S.; Myroniuk, V.; Zhurba, M.; Hamburger, T.; Stohl, A.; Balkanski, Y.; Paugam, R.; Mousseau, T.A.; Møller, A.P.; et al. Resuspension and atmospheric transport of radionuclides due to wildfires near the Chernobyl Nuclear Power Plant in 2015: An impact assessment. *Sci. Rep.* **2016**, *6*, 26062. [CrossRef] [PubMed]
8. Pazukhin, E.M.; Borovoi, A.A.; Ogorodnikov, B.I. Forest Fire as a Factor of Environmental Redistribution of Radionuclides Originating from Chernobyl Accident. *Radiochemistry* **2004**, *46*, 102–106. [CrossRef]

9. Wotawa, G.; De Geer, L.-E.; Becker, A.; D'Amours, R.; Jean, M.; Servranckx, R.; Ungar, K. Inter- and intra-continental transport of radioactive cesium released by boreal forest fires. *Geophys. Res. Lett.* **2006**, *33*, 12806. [CrossRef]
10. Evangeliou, N.; Balkanski, Y.; Cozic, A.; Hao, W.M.; Mouillot, F.; Thonicke, K.; Paugam, R.; Zibtsev, S.; Mousseau, T.A.; Wang, R.; et al. Fire evolution in the radioactive forests of Ukraine and Belarus: Future risks for the population and the environment. *Ecol. Monogr.* **2015**, *85*, 49–72. [CrossRef]
11. Yoschenko, V.; Kashparov, V.; Protsak, V.; Lundin, S.; Levchuk, S.; Kadygrib, A.; Zvarich, S.; Khomutinin, Y.; Maloshtan, I.; Lanshin, V.; et al. Resuspension and redistribution of radionuclides during grassland and forest fires in the Chernobyl exclusion zone: Part I. Fire experiments. *J. Environ. Radioact.* **2006**, *86*, 143–163. [CrossRef] [PubMed]
12. Kashparov, V.; Lundin, S.; Kadygrib, A.; Protsak, V.; Levtchuk, S.; Yoschenko, V.; Kashpur, V.; Talerko, N. Forest fires in the territory contaminated as a result of the Chernobyl accident: Radioactive aerosol resuspension and exposure of fire-fighters. *J. Environ. Radioact.* **2000**, *51*, 281–298. [CrossRef]
13. Evangeliou, N.; Eckhardt, S. Uncovering transport, deposition and impact of radionuclides released after the early spring 2020 wildfires in the Chernobyl Exclusion Zone. *Sci. Rep.* **2020**, *10*, 1–10. [CrossRef] [PubMed]
14. Talerko, M.; Kovalets, I.; Lev, T.; Igarashi, Y.; Romanenko, O. Simulation study of radionuclide atmospheric transport after wildland fires in the Chernobyl Exclusion Zone in April 2020. *Atmos. Pollut. Res.* **2021**, *12*, 193–204. [CrossRef]
15. Kuzmenkova, N.; Rozhkova, A.; Vorobyova, T. Aerosol activity measurements associated with the burning of peat materials (evacuation zone of the Bryansk Region). *J. Environ. Radioact.* **2020**, *216*, 106184. [CrossRef]
16. IRSN Information Note of 17 April 2020 "Fires in Ukraine in the Exclusion Zone Around the Chernobyl Power Station: Situation Report". Information Note NO. 3. Available online: https://www.irsn.fr/EN/newsroom/News/Documents/IRSN_Information-Report_Fires-in-Ukraine-in-the-Exclusion-Zone-around-chernobyl-NPP_17042020.pdf (accessed on 17 November 2020).
17. NASAb Sees Fires Near Chernobyl Break Out Again. Available online: https://www.nasa.gov/image-feature/goddard/2020/nasa-sees-fires-near-chernobyl-break-out-again (accessed on 1 December 2020).
18. Grell, G.A.; Peckham, S.E.; Schmitz, R.; McKeen, S.A.; Frost, G.; Skamarock, W.C.; Eder, B. Fully coupled "online" chemistry within the WRF model. *Atmos. Environ.* **2005**, *39*, 6957–6975. [CrossRef]
19. TOP Platform. Available online: http://top-platform.eu/ (accessed on 17 March 2021).
20. Pisso, I.; Sollum, E.; Grythe, H.; Kristiansen, N.I.; Cassiani, M.; Eckhardt, S.; Arnold, D.; Morton, D.; Thompson, R.L.; Zwaaftink, C.D.G.; et al. The Lagrangian particle dispersion model FLEXPART version 10.4. *Geosci. Model Dev.* **2019**, *12*, 4955–4997. [CrossRef]
21. Morrison, H.; Thompson, G.; Tatarskii, V. Impact of Cloud Microphysics on the Development of Trailing Stratiform Precipitation in a Simulated Squall Line: Comparison of One- and Two-Moment Schemes. *Mon. Weather. Rev.* **2009**, *137*, 991–1007. [CrossRef]
22. Iacono, M.J.; Delamere, J.S.; Mlawer, E.J.; Shephard, M.W.; Clough, S.A.; Collins, W.D. Radiative forcing by long-lived greenhouse gases: Calculations with the AER radiative transfer models. *J. Geophys. Res. Space Phys.* **2008**, *113*, D13103. [CrossRef]
23. Grell, G.A.; Freitas, S.R. A scale and aerosol aware stochastic convective parameterization for weather and air quality modeling. *Atmos. Chem. Phys. Discuss.* **2014**, *14*, 5233–5250. [CrossRef]
24. Chen, F.; Dudhia, J. Coupling an advanced land surface–hydrology model with the Penn State–NCAR MM5 modeling system. Part I: Model implementation and sensitivity. *Mon. Weather. Rev.* **2001**, *129*, 569–585. [CrossRef]
25. Nakanishi, M.; Niino, H. An Improved Mellor–Yamada Level-3 Model with Condensation Physics: Its Design and Verification. *Bound. Layer Meteorol.* **2004**, *112*, 1–31. [CrossRef]
26. European Centre for Medium-Range Weather Forecasts. Available online: http://www.ecmwf.int/ (accessed on 27 October 2012).
27. Sofiev, M.; Vankevich, R.; Lotjonen, M.; Prank, M.; Petukhov, V.; Ermakova, T.; Koskinen, J.; Kukkonen, J. An operational system for the assimilation of the satellite information on wild-land fires for the needs of air quality modelling and forecasting. *Atmos. Chem. Phys. Discuss.* **2009**, *9*, 6833–6847. [CrossRef]
28. Andreae, M.O.; Merlet, P. Emission of trace gases and aerosols from biomass burning. *Glob. Biogeochem. Cycles* **2001**, *15*, 955–966. [CrossRef]
29. Peckham, S.E. WRF-Chem v3.9.1.1 Emissions Guide. Available online: https://ruc.noaa.gov/wrf/wrf-chem/Emission_guide.pdf (accessed on 26 March 2021).
30. Grell, G.A.; Freitas, S.R.; Stuefer, M.; Fast, J. Inclusion of biomass burning in WRF-Chem: Impact of wild fires on weather forecasts. *Atmos. Chem. Phys.* **2011**, *11*, 5289–5303. [CrossRef]
31. European Space Agency, Sentinel 5P Description. Available online: https://sentinel.esa.int/web/sentinel/missions/sentinel-5p/ (accessed on 18 December 2020).
32. Tichý, O.; Šmídl, V.; Hofman, R.; Stohl, A. LS-APC v1.0: A tuning-free method for the linear inverse problem and its application to source-term determination. *Geosci. Model Dev.* **2016**, *9*, 4297–4311. [CrossRef]
33. Brioude, J.; Kim, S.-W.; Angevine, W.M.; Frost, G.J.; Lee, S.-H.; McKeen, S.A.; Trainer, M.; Fehsenfeld, F.C.; Holloway, J.S.; Ryerson, T.B.; et al. Top-down estimate of anthropogenic emission inventories and their interannual variability in Houston using a mesoscale inverse modeling technique. *J. Geophys. Res. Space Phys.* **2011**, *116*. [CrossRef]
34. Angevine, W.M.; Brioude, J.; McKeen, S.; Holloway, J.S. Uncertainty in Lagrangian pollutant transport simulations due to meteorological uncertainty from a mesoscale WRF ensemble. *Geosci. Model Dev.* **2014**, *7*, 2817–2829. [CrossRef]

35. Tarantola, A. *Inverse Problem Theory and Methods for Model Parameter Estimation*; Society for Industrial & Applied Mathematics (SIAM): Philadelphia, PA, USA, 2005; p. 342.
36. Karion, A.; Lauvaux, T.; Coto, I.L.; Sweeney, C.; Mueller, K.; Gourdji, S.; Angevine, W.; Barkley, Z.; Deng, A.; Andrews, A.; et al. Intercomparison of atmospheric trace gas dispersion models: Barnett Shale case study. *Atmos. Chem. Phys. Discuss.* **2019**, *19*, 2561–2576. [CrossRef]
37. Brioude, J.; Cooper, O.R.; Feingold, G.; Trainer, M.; Freitas, S.R.; Kowal, D.; Ayers, J.; Prins, E.; Minnis, P.; McKeen, S.A.; et al. Effect of biomass burning on marine stratocumulus clouds off the California coast. *Atmos. Chem. Phys. Discuss.* **2009**, *9*, 8841–8856. [CrossRef]
38. Martin, M.V.; Logan, J.A.; Kahn, R.A.; Leung, F.-Y.; Nelson, D.L.; Diner, D.J. Smoke injection heights from fires in North America: Analysis of 5 years of satellite observations. *Atmos. Chem. Phys. Discuss.* **2010**, *10*, 1491–1510. [CrossRef]
39. ECMWF: ECMWF CAMS Near-Real-Time. Available online: https://apps.ecmwf.int/datasets/data/cams-nrealtime/levtype=sfc/ (accessed on 27 August 2020).
40. NASAa: MODIS—Moderate Resolution Imaging Spectrometer. Available online: https://modis.gsfc.nasa.gov/ (accessed on 27 August 2020).
41. ECMWF: ECMWF CAMS Global Fire Assimilation System. Available online: https://apps.ecmwf.int/datasets/data/cams-gfas/ (accessed on 27 August 2020).
42. UNIAN. Kyiv Tops Air Quality Ranking as most Polluted City on April 16; Ukrainian Independent News Agency of News. Available online: https://www.unian.info/kyiv/10962650-kyiv-tops-air-quality-ranking-as-most-polluted-city-on-april-16.html (accessed on 12 October 2020).
43. BBC News. *Wildfires Blanket Kyiv in Thick Smog*; BBC: London, UK, 17 April 2020.
44. GardaWorld. *Ukraine: High. Air Quality Pollution Levels in Kyiv April 16–17*; GardaWorld: Montreal, QC, Canada, 18 April 2020.
45. U.S. EPA.: Revised Air Quality Standards for Particle Pollution and Updates to the Air Quality Index (AQI); Office of Air Quality Planning and Standards. Available online: https://www.epa.gov/sites/production/files/2016-04/documents/2012_aqi_factsheet.pdf (accessed on 20 March 2021).
46. State Statistics Service of Ukraine, Air Emissions of Some Pollutants. Available online: http://www.ukrstat.gov.ua/ (accessed on 8 January 2021).
47. Directive 2008/50/EC of 21 May 2008 on Ambient Air Quality and Cleaner Air for Europe. Available online: https://eur-lex.europa.eu/legal-content/EN/TXT/PDF/?uri=CELEX:32008L0050&from=en (accessed on 8 February 2021).
48. Protsak, V.; Voitsekhovich, O.; Laptev, G. Estimation of Radioactive Source Term Dynamics for Atmospheric Transport during Wildfires in Chernobyl Zone in Spring 2020. Ukrainian Hydrometeorological Institute (in Ukrainian). Available online: https://uhmi.org.ua/msg/fire2020/analytical.pdf (accessed on 28 April 2020).
49. Health Canada. Recommendations on dose coefficients for assessing doses from accidental radionuclide releases to the environment. In *Prepared by a Joint Working Group of Radiation Protection Bureau, Health Canada, Atomic Energy Control Board, Atomic Energy of Canada Limited*; MIC-99-03738/XAB; Health Canada: Ottawa, ON, Canada, 1999.